JACS
JOURNAL OF THE AMERICAN CHEMICAL SOCIETY
Article
pubs.acs.org/JACS

A Hybrid DNA-Templated Gold Nanocluster For Enhanced Enzymatic Reduction of Oxygen

Saumen Chakraborty,[†,∥] Sofia Babanova,[§,∥] Reginaldo C. Rocha,[†] Anil Desireddy,[†] Kateryna Artyushkova,[§] Amy E. Boncella,[†,⊥] Plamen Atanassov,*[,§] and Jennifer S. Martinez*[,†,‡]

[†]Center for Integrated Nanotechnologies, [‡]Institute for Materials Science, Los Alamos National Laboratory, PO BOX 1663, Los Alamos, New Mexico 87545, United States

[§]Center for Micro-Engineered Materials (CMEM) and Department of Chemical & Biological Engineering, The University of New Mexico, Advanced Materials Laboratory, 1001 University Blvd. SE, Albuquerque, New Mexico 87106, United States

Supporting Information

ABSTRACT: We report the synthesis and characterization of a new DNA-templated gold nanocluster (AuNC) of ∼1 nm in diameter and possessing ∼7 Au atoms. When integrated with bilirubin oxidase (BOD) and single walled carbon nanotubes (SWNTs), the AuNC acts as an enhancer of electron transfer (ET) and lowers the overpotential of electrocatalytic oxygen reduction reaction (ORR) by ∼15 mV as compared to the enzyme alone. In addition, the presence of AuNC causes significant enhancements in the electrocatalytic current densities at the electrode. Control experiments show that such enhancement of ORR by the AuNC is specific to nanoclusters and not to plasmonic gold particles. Rotating ring disk electrode (RRDE) measurements confirm $4e^-$ reduction of O_2 to H_2O with minimal production of H_2O_2, suggesting that the presence of AuNC does not perturb the mechanism of ORR catalyzed by the enzyme. This unique role of the AuNC as enhancer of ET at the enzyme-electrode interface makes it a potential candidate for the development of cathodes in enzymatic fuel cells, which often suffer from poor electronic communication between the electrode surface and the enzyme active site. Finally, the AuNC displays phosphorescence with large Stokes shift and microsecond lifetime.

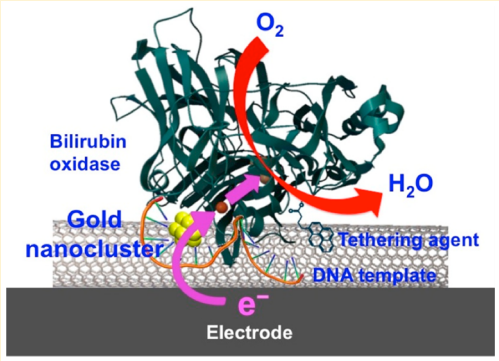

INTRODUCTION

With sources of fossil fuels dwindling, there is an urgent need to find cheap, renewable, and alternate forms of energy using naturally abundant resources such as sunlight, air, and water. Nanostructured materials and enzymatic fuel cells are showing great promise in this respect.[1] In enzymatic fuel cells, both the anodic and cathodic reactions are carried out by enzymes acting as bioelectrocatalysts. The enzymes oxidize fuels at the anode while reduction of O_2 takes place at the cathode, typically catalyzed by multicopper oxidases (MCOs).[2] The efficiency of these systems depends on how effectively the enzymes communicate with the electrode surface via direct electron transfer (DET) at potentials close to the redox potential of the enzyme.[3]

Although MCOs have been used as ORR catalysts on various electrode surfaces they suffer from low conversion efficiency primarily due to the lack of effective ET between the electrode surface and the enzyme active site. In addition, there is a need for engineering suitable material architectures that provide a large surface area for good electrical connectivity, substrate accessibility to the enzyme, and yet still retain a biocompatible environment for enzyme immobilization. Overcoming these limitations can enable widespread utilization of enzymatic fuel cells as simplified devices for single-compartment operation under neutral reaction conditions and integration into various scalable systems. To this end, gold nanoparticles (AuNPs) have been used as substrates for immobilization of laccase, which showed enhanced oxygen reduction kinetics by DET.[4] However, the electrochemical output of this system still remained poor.

Atomically precise metal nanoclusters (NCs) with a diameter of less than 2 nm and consisting of ∼2−200 atoms arranged in well-defined and stable geometric structures are showing important applications across multidisciplinary fields such as sensing, bioimaging, electronics, photovoltaics, and catalysis.[5] Because of their ultrasmall size, NCs possess discrete molecule-like electronic, optical, and electrochemical properties as well as specific packing of atoms on NC surface and the metallic core.[6] These unique electronic and structural aspects of NCs play critical roles in fine-tuning their characteristics and bestow them with size-dependent properties that are quite different from those of bulk metals, metal complexes, and metal nanoparticles.

Although bulk gold is inert,[7] gold nanoparticles (AuNPs) larger than 2 nm in diameter have been shown to possess

Received: May 22, 2015
Published: August 19, 2015

DOI: 10.1021/jacs.5b05338
J. Am. Chem. Soc. 2015, 137, 11678−11687

interesting catalytic properties when dispersed as ultrafine particles on metal oxide supports.[8] Among others, CO and hydrocarbon oxidation, hydrogenation, and reduction of nitrogen oxides and oxygen are the most notable examples where AuNPs have been employed as catalysts.[8a,9] The high catalytic activity of small Au particles compared to bulk metal has been attributed to several factors, including high surface density of low coordination number Au atoms and less electron density in small Au particles compared to bulk metal.[10] Although several studies examined the effect of NP size on catalytic activity,[8,9c,11] it was only recently discovered that the catalytically active species in CO oxidation is a bilayer of 10-atom gold nanoclusters (AuNCs), ∼ 0.5 nm in diameter.[12] Subsequently, several research groups reported catalytic activity of atomically monodisperse, ultrasmall AuNCs (<2 nm) in solution toward oxidation of organic substrates,[13] hydrogenation,[13a,14] electrocatalytic reduction of CO_2,[15] and ORR.[16] While the reported AuNCs showed a strong size effect on ORR activity, unfortunately onset potentials (E_{onset}) for ORR were low [e.g., − 0.1 V for Au_{11}, − 0.16 V for Au_{25}, − 0.2 V for Au_{55}, and −0.25 V for Au_{140} (vs Ag/AgCl)] indicating a high overpotential for the reaction.[16] In addition, these experiments were exclusively performed in alkaline media. Therefore, efficient ORR catalysts need to be designed with low overpotential and which operate under more environmentally benign aqueous conditions.

Ligands are critical for the synthesis, stabilization and control of electronic properties of metal nanoclusters.[17] Over the past decade, DNA has been increasingly used as a ligand to prepare silver,[18] copper,[19] and platinum[20] nanoclusters with interesting luminescent, detection, and catalytic properties.[5d,21] Because DNA is a natural nanoscale material with strong affinity for metal cations,[22] DNA can template and localize metals to form and stabilize NCs.[23] In addition, exquisite control of NC size and the resulting electronic and optical properties has made DNA a natural ligand choice for NC synthesis and their various applications. Finally, the chemistry of DNA-templated NCs can be performed in water and neutral conditions, which is a green and desirable method for technology development as opposed to organic solvents or acidic/alkaline reaction conditions.

Using these advantages of DNA as a ligand for NC synthesis having well-defined materials architectures, and with the wide variety of catalytic applications of AuNCs, we set out to synthesize stable AuNCs using DNA as the ligand and investigate their applications as facilitators of ET in enzymatic fuel cells. While a few examples of DNA-templated gold nanoclusters have been reported,[24] their potential applications have been unexplored due to a lack a thorough characterization. We hypothesize that due to the small size, electrochemical activity and unique properties of the AuNCs the DNA-templated AuNC could facilitate ET to the enzyme active site where reduction of O_2 takes place and thus lower the overpotential while increasing the electrocatalytic current density for ORR.

Herein we report synthesis and thorough characterization of a new DNA-templated AuNC. We demonstrate the application of this novel material in enzyme-based biofuel cells as facilitator of ET at the enzyme-electrode interface. Composites of the AuNC integrated with carbon nanotubes (CNTs) and bilirubin oxidase (BOD) were immobilized on electrode surfaces for ORR assays. Bilirubin oxidase from *Myrothecium verrucaria* was chosen as the desired MCO due to its known structure and ready commercial availability. BOD has an ET T1 Cu site, and a catalytic T2/T3 Cu site where the reduction of O_2 takes place.[25] The relatively high redox potential of BOD[26] makes it advantageous for improving its performance toward electrocatalytic oxygen reduction. This unique application of the AuNC as facilitator of ET for ORR demonstrates the beneficial aspects of NC size effects and opens up many possibilities for technology developments in the long term, including biosensors, actuators, and biological fuel cells.

RESULTS AND DISCUSSION

Electronic and Secondary Structural Changes during AuNC Formation. DNA-templated AuNC was synthesized according to Scheme 1 (see Materials and Methods for details).

Scheme 1. Synthetic Scheme of the AuNC[a]

[a]Black curves represent DNA backbone, pink lines represent DNA bases, individual yellow spheres represent Au(III), while AuNC is shown as the cluster of yellow spheres.

To monitor electronic changes occurring during AuNC formation, UV−vis absorption spectroscopy was employed. Incubation of DNA with Au(III) causes a red shift in the λ_{max} of DNA from 261 to 266 nm (Figure 1), indicating complexation of Au(III) ions to the functional groups of DNA (likely binding to nucleobases by Lewis acid−base interactions). Upon reduction of Au(III) and formation of nanoclusters, further spectral changes occur and the λ_{max} subsequently blue-shifts from 266 to 264 nm (Figure 1), indicating different electronic transitions in the DNA when the AuNC is formed, compared to

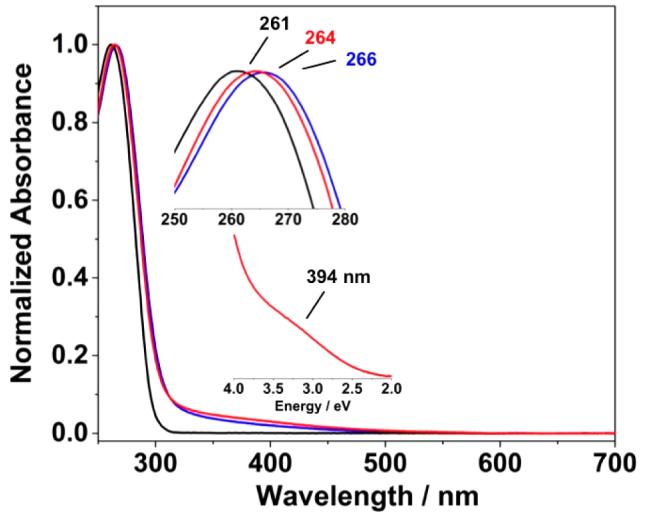

Figure 1. Electronic changes occur during the AuNC formation. UV−vis absorption spectra of solutions containing 15 μM DNA (black line), 15 μM DNA + 225 μM $HAuCl_4$ (blue line), and the as synthesized AuNC (red line) in 20 mM phosphate buffer, 1 mM $Mg(OAc)_2$, pH 7. The top inset shows the clear shifts in the λ_{max} of DNA upon Au(III) complexation and subsequent AuNC formation. The bottom inset shows the spectrum of AuNC after subtraction of the absorption by DNA alone.

DOI: 10.1021/jacs.5b05338
J. Am. Chem. Soc. 2015, 137, 11678−11687

the initial Au(III)-DNA complex. Similar trend in spectral shifts was observed during the formation of a DNA-templated AgNC.[18a] Upon subtracting the DNA contribution from the spectrum of AuNC, the presence of a broad shoulder centered ~394 nm (3.15 eV) was observed (Figure 1, inset). Discrete molecule-like electronic transitions in the range 330−390 nm have been reported for small gold clusters (e.g., $Au_{10-12}SG_{10-12}$,[27] $Au_{11}C_{12}$,[28] $Au_{13}[PPh_3]_4[S-(CH_2)_{11}CH_3]_2Cl_2$,[29] $Au_{13}[PPh_3]_4[S(CH_2)_{11}-CH_3]_4$,[29] and Au_8PAMAP[30]), the spectral features of which depend on various factors such as ligand type, geometry, core size, and oxidation states of the clusters.[31] Therefore, it is likely that some or all of these factors contribute to the broadness of this shoulder feature in the spectra of the DNA-templated AuNC reported here.

To probe whether secondary structural changes occur in the DNA molecule during AuNC formation, we used circular dichroism spectroscopy, which is sensitive to changes in the chirality of ribose sugars. DNA alone shows two positive CD bands at 279 and 219 nm and two negative bands at 244 and 209 nm (Figure 2), respectively. Similar to the electronic

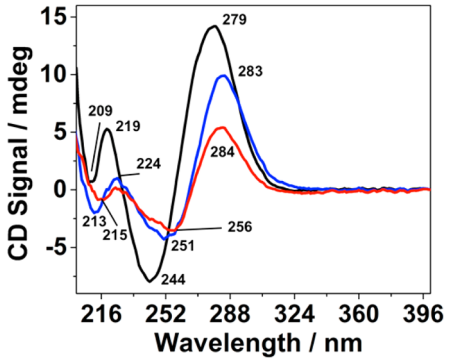

Figure 2. Secondary structural changes occur during the AuNC formation. CD spectra of solutions containing 100 μM DNA (black line); 150 μM DNA + 2250 μM $HAuCl_4$ (blue line); and the synthesized AuNC (red line).

absorption spectrum, the CD spectrum also changes upon Au(III) complexation to DNA and subsequent reduction of Au(III) leading to the formation of AuNC (Figure 2), suggesting secondary structural changes in the DNA during these processes. Spectral shifts in both the absorption and CD spectra suggest changes in the electronic transitions and secondary structure of DNA upon Au(III) coordination and subsequent cluster formation process.

The AuNC Is a Small Cluster with ~7 Au Atoms. Transmission electron microscopy (TEM) analysis was further performed to determine the size of AuNC. The TEM micrograph of the AuNC shows the presence of many small particles with average size of ~0.9 nm in diameter (Figure 3), which is characteristic of small gold clusters.[32] The observed apparent polydispersity due to the presence of a few larger particles is originating from electron beam damage of the nanoclusters that causes sintering of the metal, which is a widely observed phenomenon while imaging such small particles.[33] The TEM image further proves that the material under study is truly nanocluster in nature and not plasmonic AuNPs (>2 nm in diameter). To determine the number of Au atoms present in the AuNC we performed MALDI-MS of the DNA and the AuNC in both negative and positive ionization

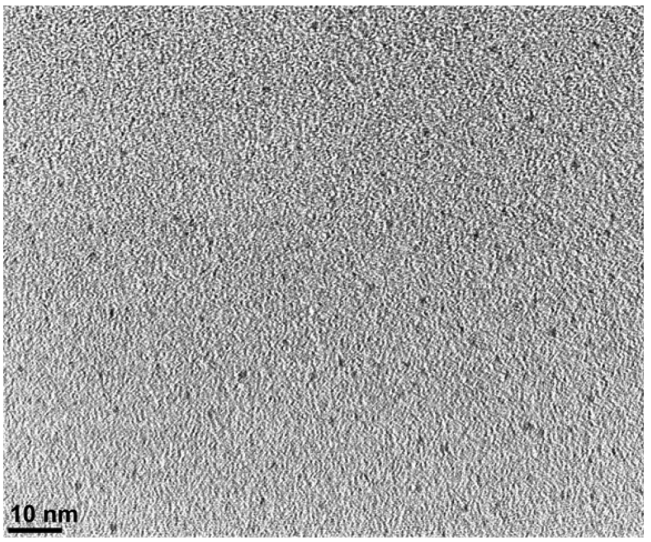

Figure 3. TEM shows small gold clusters. TEM image of the AuNC showing the presence of small clusters with average size of ~0.9 nm in diameter. Scale bar: 10 nm.

modes. The observed molecular weights of the AuNC are 10 400 and 10 524 Da in negative and positive ionization modes, respectively; while those of DNA are 9054 and 9196 Da (Figure S1). After subtracting the corresponding DNA, the total number of Au atoms present in the AuNC was calculated to be ~7 in both negative and positive ionization modes, suggesting that the AuNC is a 7-atom cluster ligated by a single DNA molecule. Although the widths of the AuNC peak in the MALDI spectra are greater than that of DNA alone, it is likely that the extent of ionization of DNA and AuNC are different, giving rise to differences in the observed resolution. Additionally, given that even well characterized and atomically precise thiol-protected gold clusters exhibit broad MALDI spectra, the observation of such spectral broadening in the DNA-protected AuNC is not unusual.[16,34] The observed number of Au atoms in the AuNC is less than the initial molar ratio of 1:15 (DNA:Au) as some of the added Au(III) produces plasmonic Au particles upon reduction (see Materials and Methods). Furthermore, it is commonly found for DNA-templated nanoclusters that the metal−ligand stoichiometry of the reaction mixture is not maintained in the final product.[18a,c,d,35]

To further probe the composition of the AuNC, we performed energy dispersive X-ray spectroscopy (EDX) analysis to calculate the Au atom count (Figure S2). From intensities of the Au Lα (9.712 keV) and P Kα (2.013 keV) lines, the atomic percentages of P and Au were obtained. From this analysis the number of Au atoms present in one DNA molecule was found to be ~7 (see Materials and Methods for details). While small clusters of 3−13 Au atoms protected by ligands other than DNA have been reported,[36] a rigorous analysis of AuNC size and atom count has not been previously performed for any DNA-templated AuNC.

To find out the number of gold atoms present in the AuNC, we inspected the P 2p and Au 4f X-ray photoelectron spectra (XPS). From these data the relative atomic % of P and Au are found to be 3.1 and 0.74%, respectively. Analysis of the data yielded a ~ 7 atom Au cluster (see Materials and Methods), which is also consistent with the MALDI-MS and EDX data (vide supra) in suggesting the presence of ~7 Au atoms in the AuNC.

DOI: 10.1021/jacs.5b05338
J. Am. Chem. Soc. 2015, 137, 11678−11687

AuNC Is a Mixed-Valence Cluster. Next, we used XPS to investigate whether the clusters possessed only Au(0) or both Au(0) and Au(I) oxidation states. The Au 4f XPS spectrum of the AuNC sample (Figure 4, blue line) shows an intense and sharp peak at ~85 eV, a less intense and broader peak at ~88.5 eV, and a small peak at ~91 eV. The sharp peak at ~85 eV corresponds to the Au $4f_{7/2}$ component and the other two peaks correspond to the Au $4f_{5/2}$ components. Deconvolution of the spectral envelope yielded individual Au species corresponding to different oxidation states. The Au $4f_{7/2}$ line consists of contributions from a Au(0) species at 84.2 eV (Figure 4, black line) and a Au(I) species at 85 eV (Figure 4, green line) present at a relative population of 0.27:1, respectively. These data therefore show that the DNA-templated AuNC has characteristics of nanoclusters with both Au(0) and Au(I) oxidation states (i.e., a mixed-valence cluster). In addition to Au(I) and Au(0), a small fraction of residual Au(III) may still remain in the sample as observed from the Au $4f_{7/2}$ peak at 87.1 eV (red dotted line).

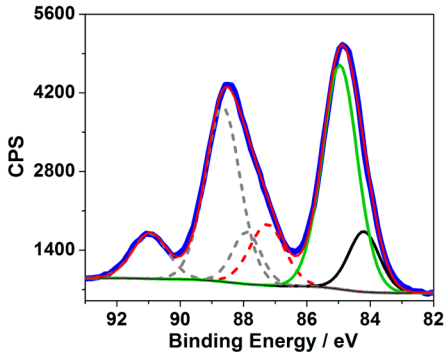

Figure 4. The AuNC consists of both Au(0) and Au(I) oxidation states. Au 4f XPS spectra showing the presence of both Au(0) and Au(I). Blue line: experimental spectrum; red solid line: fitted spectrum; black line: Au $4f_{7/2}$ component of Au(0); green line: Au $4f_{7/2}$ component of Au(I); red dotted line: Au $4f_{7/2}$ component of residual Au(III); gray lines: corresponding Au $4f_{5/2}$ components.

Upon the basis of NMR and EXAFS data of Ag-coordinated DNA as well as Raman data on DNA-bound metal ions it is suggested that metals bind to DNA through the N7 of purines and N3 of pyrimidines.[18a,37] Here, we examined the N 1s XPS data to gain insight into whether nitrogen atoms of DNA bases are ligating to Au in the AuNC. The N 1s XPS data show that the speciation of nitrogen has changed in the AuNC sample compared to metal-free DNA (Figure S3). Specifically, the relative ratio of amine (398.8 eV) and amide (400.3 eV) peaks changes between the DNA and the AuNC samples. In addition, protonated nitrogen species (401.3 eV) from the DNA bases changes significantly when the AuNC is formed. Measuring the pH of the DNA-only and the AuNC samples (both at pH ~ 7.0) ensured that deprotonation of the nitrogen was not due to a difference in pH. Although the identity of specific DNA bases that bind to the Au cannot be determined, these data suggest that the AuNC is preferentially formed with ligation from the nitrogens of the DNA bases, for which the chemical environment changes upon binding of gold.

The AuNC Displays Large Stokes Shift with Microsecond Lifetime. Having established the size and composition of DNA-templated AuNC, we explored whether it was luminescent. At relatively high concentrations (~1 mM), the AuNC showed luminescence with an emission peak at 650 nm (Figure 5, blue line) resulting from a photoexcitation at 470 nm (Figure 5, green line). The large Stokes shift of 180 nm suggests that the primary origin of this emission is phosphorescence, which was supported by lifetime measurements. Analysis of the luminescence decay curves showed the presence of two emission components with microsecond lifetimes [4.2 μs (89%) and 0.6 μs (11%); Figure S4)]. Such large Stokes shifts and microsecond lifetimes have also been observed in luminescent Au(I) complexes,[27a,38] as well as in ligand-protected luminescent AuNCs with glutathione (AuNC@GSH: λ_{ex} = 365 nm, λ_{em} = 610 nm),[27a] D-penicillamine (AuNC@D-Pen: λ_{ex} = 400 nm, λ_{em} = 610 nm),[5a] and dihydrolipoic acid (AuNC@DHLA: λ_{ex} = 490 nm, λ_{em} = 650 nm).[5b,c] A quantum yield of 2.6×10^{-3} determined using $[Ru(bpy)_3]Cl_2$ ($\phi = 2.8 \times 10^{-2}$ in air-saturated aqueous solution)[39] suggests that the AuNC is weakly luminescent. However, the luminescence quantum yield is comparable to or, in some cases, several orders of magnitude greater than those of ligand-protected gold clusters with ligands such as glutathione ($\phi = 3.5 \times 10^{-3}$),[5f] tiopronin ($\phi = 3 \times 10^{-3}$),[40] dimarcaptosuccinic acid ($\phi = 1 \times 10^{-6}$),[41] and dodecanethiol ($\phi = 4.4 \times 10^{-5}$, $< 3 \times 10^{-7}$).[42]

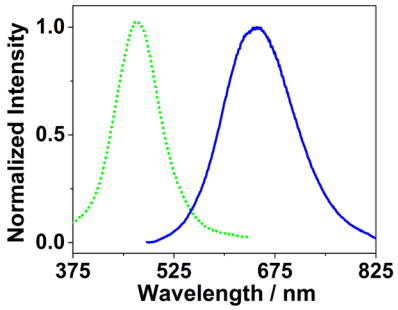

Figure 5. The luminescent AuNC shows large Stokes shift. Excitation spectrum (green line; λ_{em} = 650 nm) and emission spectrum (blue line; λ_{ex} = 470 nm) of ~1 mM AuNC in 20 mM phosphate buffer, 1 mM $Mg(OAc)_2$, pH 7.

It has been recently proposed that the origin of luminescence in AuNCs can be attributed to the presence of large fraction of Au(I), and that the AuNCs can be present as a mixed-valence species lying in between luminescent Au(I) complexes and nonluminescent AuNPs.[43] To test whether the luminescence in the DNA-templated AuNC is due to the presence of Au(I), the spectral changes were monitored upon reducing the Au(I) in the luminescent AuNC. Addition of $NaBH_4$ (1.0 equiv with respect to gold concentration) to a solution of AuNC caused a significant decrease in emission at 650 nm, with ~90% loss of the initial luminescence (Figure S5). This observation suggests that the luminescence of DNA-templated AuNC is associated with the presence of Au(I). Consequently, no luminescence was observed when $NaBH_4$ was used instead of dimethylamine borane (DMAB) as the reductant during the AuNC synthesis. This result corroborates the hypothesis that the presence of Au(I) is critical to the appearance of luminescence in the DNA-templated AuNC.

The AuNC Is Electrochemically Active. Electrochemical properties of the AuNC were assessed by cyclic voltammetry (CV) and differential pulse voltammetry (DPV). Although the CV scans show two poorly defined redox processes (Figure 6a, marked as *), DPV shows two resolved processes occurring at 0.155 and 0.210 V vs Ag/AgCl, respectively (Figure 6b). From

DOI: 10.1021/jacs.5b05338
J. Am. Chem. Soc. 2015, 137, 11678−11687

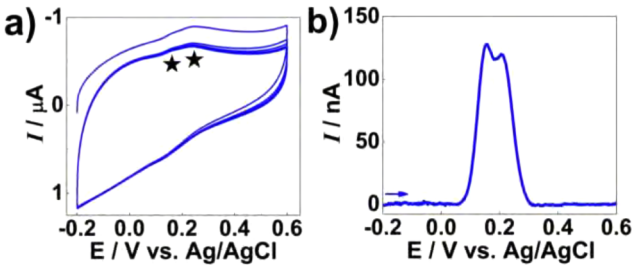

Figure 6. The AuNC is electrochemically active. (a) CV scans at a scan rate of 50 mV/s. (b) DPV scans in the anodic direction (pulse period = 250 ms, pulse width = 25 ms, amplitude = 25 mV, increment = 2 mV). The concentration of sample solutions were ~0.5 mM AuNC in 50 mM phosphate buffer, 1 mM $Mg(OAc)_2$, pH 7.

electrochemical studies of monolayer protected AuNCs of various sizes (e.g., $Au_{25}(SC6)_{18}$,[44] $Au_{38}(SC_2H_4Ph)_{24}$,[45] and $Au_{67}(SR)_{35}$[46]), multiple redox processes have been assigned to sequential one-electron oxidation/reduction of the various charge states of the clusters. Here, the two closely spaced potentials are likely associated with two successive one-electron oxidations at the AuNC (i.e., two Au(0)/Au(I) processes). As with polynuclear charge-transfer molecular complexes, it is possible that the first oxidation introduces an electronic perturbation (in addition to the change in overall charge) that causes the shift of the second process.[47]

Oxygen Reduction Activity of AuNC/BOD Composites. Motivated by the electrochemical activity and small size of the AuNC, we investigated whether these unique properties can be utilized for enhanced ET between the electrode and the enzyme. BOD was used as an enzyme of choice as it is a well-known enzyme for catalyzing ORR. To test our hypothesis, the AuNC was integrated with BOD by using single-walled carbon nanotubes (SWNTs) as a support material. SWNT was dispersed via tetrabutylammonium bromide (TBAB) modified Nafion. TBAB modification causes exchange of the proton from Nafion sulfonic acid group and affords the TBAB salt of Nafion.[48] This modification results in an increase in the pore size of the Nafion polymer allowing easy diffusion of substrates and ions to the enzyme active site, and reduces acidity of Nafion, thus making it a more biocompatible polymer for immobilization of the enzyme on the electrode surface.[48] DNA-templated AuNC was then mixed with the suspension of SWNT to allow for stacking of the DNA to the SWNT by noncovalent $\pi-\pi$ stacking interactions. Next, 1-pyrenebutanoic acid succinimidyl ester (PBSE) was added to the mixture followed by BOD and incubated overnight. While the pyrene groups of PBSE tether to the SWNT by $\pi-\pi$ stacking interactions, the succinimidyl ester groups covalently attach to the surface amine groups of the BOD via succinimidyl ester-amine cross-linking chemistry to prepare the final composite material BOD-AuNC/SWNT. A schematic of the composite preparation method is shown in Scheme 2. Control composites consisting of (i) SWNT and BOD (BOD/SWNT), (ii) SWNT, DNA alone, and BOD (BOD-DNA/SWNT), (iii) SWNT, plasmonic Au particles (side product in the AuNC synthesis) and BOD (BOD-plasmonic Au/SWNT) were prepared using similar methods as above but without the AuNC. For electrocatalytic ORR measurements the samples were drop cast on a rotating disk electrode (RDE), dried, and their oxygen reduction activity was tested using linear sweep voltammetry (LSV) with a scan rate of 10 mV/s.

Scheme 2. Composite Preparation for ORR Assays[a]

[a]AuNC: gold nanocluster, PBSE: 1-pyrenebutanoic acid succinimidyl ester, BOD: bilirubin oxidase, RDE: rotating disk electrode, RE: reference electrode, CE: counter electrode.

First, we performed electrochemical measurements of BOD-AuNC/SWNT composite under O_2 depleted, and dissolved O_2 conditions. Under O_2-depleted conditions (Figure S6, black line), very low current was observed due to the small amount of oxygen present in the electrolyte solution (~0.66 mg/L). In the presence of dissolved atmospheric O_2 (~6.91 mg/L) moderate current was observed for the enzymatic ORR (Figure S6, red line). Below ~1.040 V (vs RHE), the current density decreased because the reaction was limited by the availability of O_2 in the electrolyte solution.

We next tested electrocatalytic activity of BOD-AuNC/SWNT and two control composites (BOD/SWNT and BOD-DNA/SWNT) in O_2-saturated buffer. The BOD/SWNT control composite (Figure 7, black line) showed catalytic

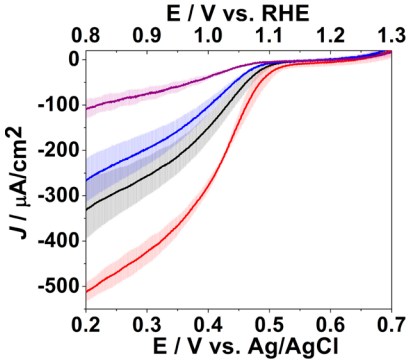

Figure 7. LSV of BOD-plasmonic Au/SWNT (purple line); BOD-DNA/SWNT (blue line); BOD/SWNT (black line); and BOD-AuNC/SWNT (red line) composite materials in O_2-saturated 0.1 M phosphate buffer (pH 7.5). Traces and shaded areas represent the average and standard deviations, respectively, of the data obtained by testing three different samples, prepared and tested independently. Scan rate = 10 mV/s; rotation rate = 1600 rpm. [Note: Although potentials were measured vs Ag/AgCl, here they are converted and referred to against RHE due to its appropriateness to ORR; for the conversion, $E_{RHE} = E_{Ag/AgCl} + 0.059 \times pH + E^0_{Ag/AgCl}$ ($E^0_{Ag/AgCl} = 0.197$ V)].

current with E_{onset} of ~1.150 V (vs RHE), apparent $E_{1/2}$ of ~1.055 V, and current density of ~257 $\mu A/cm^2$ [Δi measured as the difference in current between E_{onset} and the reductive current at 0.940 V] (Table 1). In contrast, the BOD-DNA/SWNT control composite (Figure 7, blue line) showed a cathodically shifted E_{onset} at ~1.125 V. In addition, $E_{1/2}$ decreased to ~1.040 V in conjunction with the catalytic

DOI: 10.1021/jacs.5b05338
J. Am. Chem. Soc. 2015, 137, 11678−11687

Table 1. Electrochemical Results Obtained from LSVs in O_2-Saturated Buffer[a]

sample	E_{onset} V vs Ag/AgCl (V vs RHE)	$E_{1/2}$ V vs Ag/AgCl (V vs RHE)	Δi[b] (μA/cm^2)
BOD-plasmonic Au/SWNT	0.480 (1.120)	0.355 (0.995)	74
BOD-DNA/SWNT	0.485 (1.125)	0.400 (1.040)	197
BOD/SWNT	0.510 (1.150)	0.415 (1.055)	257
BOD-AuNC/SWNT	0.525 (1.165)	0.430 (1.070)	412

[a]Potentials vs RHE in parentheses. [b]Δi is the differential current between the onset potential (E_{onset}) and the reductive current at 0.940 V.

current density, which was reduced to ~197 μA/cm^2 from ~257 μA/cm^2 observed in the BOD/SWNT composite (Table 1). These results suggest that DNA can hinder the interfacial ET from the electrode to the enzyme and thus be detrimental to the ORR (supported by lower current densities with increase in DNA concentration, Figure S7). Remarkably, the presence of the AuNC caused significant changes in the ORR profile displayed by the BOD-AuNC/SWNT composite (Figure 7, red line). First, E_{onset} was anodically shifted to ~1.165 from ~1.150 V observed using the BOD/SWNT sample, corresponding to a positive shift of ~0.015 V. Second, the electrocatalytic current density was increased to ~412 μA/cm^2, an increase of ~155 μA/cm^2 compared to BOD/SWNT composite. Finally, the $E_{1/2}$ increased to ~1.070 V from that of ~1.055 V observed using BOD/SWNT (Table 1). These exciting results, therefore, suggest that the presence of AuNC enhances the ORR activity of the enzyme by lowering the overpotential by a significant ~0.015 V with concomitant increase in the kinetics of the reaction, which leads to higher catalytic current densities.

To investigate whether such enhancement of ORR activity by the AuNC is specific to nanoclusters, we performed LSV of BOD-plasmonic Au/SWNT control composite consisting of the SWNT, plasmonic Au particles (side product in the cluster synthesis), and BOD. This data (Figure 7, purple line) shows that the E_{onset} shifts to ~1.120 V as compared to ~1.165 V observed in the presence of AuNC. Further, the $E_{1/2}$ also significantly shifts to a lower potential of ~0.995 V as compared to ~1.070 V obtained with the BOD-AuNC/SWNT composite with a concomitant reduction of electrocatalytic current density at the electrode (~74 μA/cm^2 compared to ~412 μA/cm^2 observed with AuNC). These data, therefore, convincingly suggest that the enhancement of ORR (by lowering the overpotential by ~0.015 V) as well as the enhancement of catalytic current densities in the presence of AuNC is unique to nanoclusters, which improved kinetics and thermodynamics of ORR. Such enhancement of ORR activity by the AuNC is unprecedented. The likely mechanism by which the AuNC enhances the ORR performance is by facilitating the ET between the electrode surface and the enzyme active site through a more effective electronic communication. These findings suggest that employment of the AuNC as an enhancer of ET between the electrode surface and the enzyme active site can potentially remove a significant barrier in enzymatic fuel cells, which often suffer from poor performance due to a lack of electronic communication between the electrode and the enzyme active site.

While the E_{onset} of the BOD-AuNC/SWNT composite is comparable (Table 1) to that of a BOD on air breathing gas diffusion electrode (GDE) (1.160 V vs RHE), the observed apparent $E_{1/2}$ in the current system (Table 1) is higher than that of the GDE (0.920 V vs RHE).[49] In addition, the BOD-AuNC/SWNT composite showed higher E_{onset} and $E_{1/2}$ compared to many reported in literature including BOD on spectrographic graphite (E_{onset} = 1.136 V, $E_{1/2}$ = 1.036 V vs RHE),[50] and BOD on CNTs (E_{onset} = 1.149 V, $E_{1/2}$ = 0.950 V vs RHE).[51] The present system also displays better thermodynamic parameters (Table 1) compared to many Pt-based materials. For example, platinum nanoparticles of various sizes (3−7 nm) reduced O_2 with E_{onset} = 0.870−0.920 V and $E_{1/2}$ = 0.750 V vs RHE,[52] platinum nanoclusters and graphene oxide composites (Pt_n/gDNA-GO) showed E_{onset} = 1.010 V and $E_{1/2}$ = 0.900 V vs RHE,[20b] Pt and Pt/Pd nanotubes as well as graphene supported Pt and Pd catalysts and Pt/Pd nanodendrites showed ORR with $E_{1/2}$ = 0.850−0.900 V vs RHE.[53] Furthermore, a recently reported Co_3O_4 nanocrystals on graphene showed ORR activity with E_{onset} = 0.880 V and $E_{1/2}$ = 0.790−0.830 V vs RHE.[54]

Further evidence of this unique role of AuNC was obtained from ORR currents measured using a different electrode design. In this case, the electrode material (multiwalled Bucky paper (MWBP)) was first soaked in AuNC solution, followed by PBSE and BOD for the immobilization of the various components (see Materials and Methods for details). The modified MWBP was then placed on a glassy carbon cap electrode and the electrode performance toward ORR was monitored in O_2-saturated buffer by measuring potentiostatic polarization curves. The sample containing both AuNC and BOD caused an increase in the ORR current density to ~735 μA/cm^2 (Figure 8, red line) from that of ~493 μA/cm^2

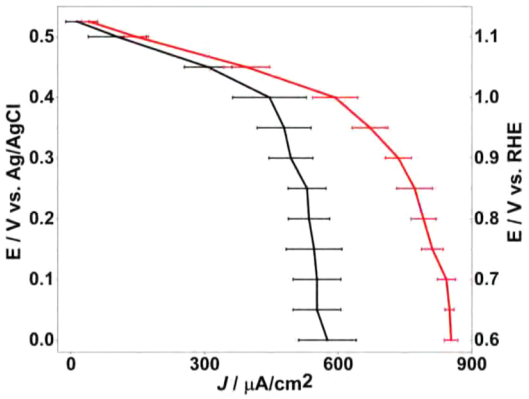

Figure 8. The AuNC enhances ORR by BOD. Potentiostatic polarization curves for BOD/MWBP (black line); and BOD-AuNC/MWBP (red line) carried out in 0.1 M phosphate buffer (pH 7.5). Standard deviations were calculated from data obtained by testing three different samples, prepared and tested independently.

obtained using BOD alone (Figure 8, black line), amounting to an increase in current density of ~50%. Therefore, these results also demonstrate that the AuNC is enhancing the performance of BOD by acting as a facilitator of the ET between the electrode surface and the enzyme active site.

Mechanistic Insight on 4e$^-$ vs 2e$^-$ Reduction. To understand whether the presence of the AuNC perturbs the mechanism of ORR by BODs with regards to 2e$^-$ vs 4e$^-$ processes, we performed mass and charge balance analysis of

DOI: 10.1021/jacs.5b05338
J. Am. Chem. Soc. 2015, 137, 11678−11687

rotating ring disk electrode (RRDE) data obtained using the BOD-AuNC/SWNT composite in O_2-saturated buffer (Figure S8). From this analysis the number of electrons (n) transferred during O_2 reduction can be calculated using the following equation:

$$n = \frac{4}{1 + \left(\frac{i_R}{\eta * i_D}\right)} \quad (1)$$

where i_R is the ring current, i_D is the disk current, and η is the collection efficiency at the electrode.[55] For RRDE, the collection efficiency is known to be 37%. The calculated number of electrons transferred during O_2 reduction by BOD-AuNC/SWNT composite was found to be 3.9 ± 0.1. This result indicates that less than 3% of O_2 was partially reduced by $2e^-$ to H_2O_2 ($O_2 + 2e^- + 2H^+ \rightarrow H_2O_2$), while almost all of O_2 was reduced to H_2O by a $4e^-$ reduction process ($O_2 + 4e^- + 4H^+ \rightarrow 2H_2O$). These observations lead to the conclusion that the presence of the AuNC did not perturb the mechanism of O_2 reduction by BOD,[56] and that the BOD-AuNC/SWNT composite material cleanly reduced O_2 to H_2O with minimal production of reactive oxygen species (ROS).

CONCLUSIONS

In conclusion, a new DNA-templated AuNC has been synthesized and thoroughly characterized. While the TEM, MALDI, EDX, and XPS analyses show that the AuNC is ∼1 nm in diameter and consists of ∼7 Au atoms, XPS also suggests the presence of both Au(0) and Au(I) oxidation states. The AuNC shows weak photoluminescence with microsecond lifetime and large Stokes shift. The observed phosphorescence can be attributed to the presence of high fraction of Au(I) in the cluster. The AuNC is electrochemically active and enhances the performance of BOD catalyzed enzymatic ORR by lowering the overpotential by ∼15 mV, and improving the electronic communication between the electrode and the enzyme active site. RRDE analysis showed that the presence of the AuNC did not perturb the mechanism of O_2 reduction, as the BOD-AuNC/SWNT composite material cleanly reduced O_2 to H_2O in a $4e^-$ pathway. Furthermore, we show that the enhancement of ORR activity is unique to nanoclusters and not to plasmonic gold nanoparticles. This unique role as ET enhancers at the enzyme-electrode interface makes the new AuNC as a potential candidate for the development of cathodes for enzymatic fuel cells, thus lifting a critical methodological barrier in biofuel cell design.

MATERIALS AND METHODS

Synthesis and Purification of the AuNC. In a typical synthesis, 15 μM single-stranded DNA (IDT, standard desalting) of sequence ACCCGAACCTGGGCTACCACCCTTAATCCCC was mixed with 225 μM $HAuCl_4.3H_2O$ (Sigma-Aldrich, ≥ 99.9% trace metals basis) in a solution of 20 mM phosphate buffer (pH 7), 1 mM $Mg(OAc)_2$ (Fisher Scientific) and equilibrated for 24 h with inverted mixing at room temperature (RT, 23 ± 2 °C). After equilibration, the solution became yellow. Reduction of Au(III) was initiated by addition of 2.25 mM dimethylamine borane (DMAB, Sigma-Aldrich) followed by equilibration at RT for 16 h. At this point, a purple solution was formed indicating the presence of plasmonic Au particles. This solution was then purified by spin filtration using 30 kDa MWCO membranes (Millipore). A yellow solution of the AuNC was collected in the filtrate while the plasmonic Au particles were retained in the membrane. The AuNC solution was stored at 4 °C before further use. Whenever necessary, the as-synthesized AuNC was concentrated using 10 kDa MWCO membranes. The highest yield of AuNC was obtained at a maximum reaction volume of ∼5 mL. At higher reaction volumes the yield of the AuNC significantly decreased and plasmonic Au particles were formed at a greater extent. For energy dispersive X-ray spectroscopy (EDX) measurements (see below) and to determine the P 2p atomic % from XPS, the AuNC was synthesized in a solution of 50 mM NH_4OAc buffer (pH 5.5), 1 mM $Mg(OAc)_2$ to avoid error in measuring the relative ratio of Au:P arising from the presence of P in phosphate buffer.

UV−Vis and Fluorescence Spectroscopy. UV−vis spectra were collected at RT using a Cary 5000 (Agilent) UV−vis NIR spectrophotometer. Fluorescence spectra were collected using wither a Cary Eclipse spectrophotometer or a Horiba Jobin Yvon Fluoromax 4 spectrofluorometer, with an excitation/emission band-pass of 5 nm. In lifetime measurements, the spectrofluorometer was coupled with a time-correlated single photon counting (TCSPC) system from Horiba Jobin Yvon. The apparatus was equipped with a pulsed laser diode source (NanoLED) operating at 1 MHz and with excitation centered at 452 nm. Analysis of fluorescence decay profiles was performed with the Horiba DAS6 software. All measurements were performed at RT. Quantum yield was determined by the gradient method,[57] using $[Ru(bpy)_3]Cl_2$ in air-saturated aqueous solution as the standard (λ_{em} = 625 nm; $\phi = 2.8 \times 10^{-2}$).[39] The excitation wavelength (λ_{ex}) was 470 nm, and the absorbance of both standard and AuNC sample solutions was maintained in the 0.03−0.1 range.

CD Spectroscopy. CD spectra were collected on a JASCO instrument using a 1 mm path length cuvette. Three scans were collected for each sample.

TEM Imaging. Bright-field transmission electron microscopy (TEM) analysis of the AuNC was performed using a FEI Tecnai F30 instrument operating at 200 kV acceleration voltage. A thin carbon-coated (carbon film thickness <10 nm) copper TEM grid (Pacific Grid-Tech, 300 mesh, 3.05 mm O.D., hole size: ∼ 63 μm) was soaked in as-synthesized AuNC solution for 2 h and air-dried before imaging.

MALDI-MS. MALDI data were collected on ABSciex 4800 Plus TOF/TOF MALDI mass spectrometer using both DNA and AuNC samples in both positive and negative ion modes with sinapinic acid (Sigma-Aldrich) as matrix. The AuNC was synthesized using the same DNA stock solution, which was used for MALDI-MS analysis of the DNA-only sample.

EDX Measurements. Energy dispersive X-ray spectroscopy (EDX) data were collected at 30 kV acceleration voltage using a FEI Quanta 400 FEG-E-SEM instrument equipped with an EDX system (EDAX Inc.). Data processing was performed using Genesis software. A concentrated sample (∼1−2 mM) of the AuNC synthesized in NH_4OAc buffer was drop cast and dried on carbon tape. The ratio of gold to phosphorus in the DNA backbone was calculated based on the total atomic % of these two elements determined from the intensities of the Au Lα (9.712 keV) and P Kα (2.013 keV) lines in the EDX spectra of the sample. Contribution from spectral overlap of the Au M line (2.120 keV) to the P Kα line was subtracted. The atomic percentages of these two elements were calculated to be 14 and 59.2, respectively. The total atomic percentage of phosphorus present in the DNA was then used to calculate the number of DNA molecules, determined to be 1.9 (59.2/31) by taking the contributions from 31 P atoms (in this study, the DNA is 31 nucleotides long). As nanoclusters are formed by a single DNA molecule, the number of Au atoms present in the AuNC was found to be ∼7.4 ± 1.0 (14/1.9).

XPS Measurements and Processing. Samples were drop cast on mica surface and air-dried before measurements. XPS measurements were performed with a Kratos Axis Ultra DLD X-ray photoelectron spectrometer using a monochromatic Al Kα source operating at 225 W. The data were acquired from 3 different areas in the sample. Survey and high resolution C 1s, O 1s, N 1s, and Au 4f were acquired at 80 and 20 eV pass energy, respectively. Standard operating conditions for charge compensation were: bias voltage of 3.1 V, filament voltage of −1.0 V, and filament current of 2.1 A. Data analysis and quantification were performed using the CasaXPS software. A linear background was

DOI: 10.1021/jacs.5b05338
J. Am. Chem. Soc. 2015, 137, 11678−11687

used for C 1s, N 1s, O 1s, and Shirley background for Au 4f spectra. All of the spectra were charge referenced to the C 1s at 284.7 eV. Quantification utilized sensitivity factors that were provided by the manufacturer. A 70% Gaussian/30% Lorentzian (GL (30)) line shape was used for the curve fittings.

Atomic % of P and Au obtained from P 2p and Au 4f XPS data were found to be 3.1% and 0.74%, respectively. Upon normalizing the atomic % of P to 1 DNA molecule (which has 31 nucleotides and thus 31 P atoms), we obtain 0.1 as the normalization factor (3.1/31 = 0.1). After normalizing the atomic % of Au with this normalization factor, the number of Au atoms present in the AuNC is thus calculated to be 7.4 (0.74/0.1 = 7.4).

Electrochemistry. Cyclic voltammetry (CV) and differential pulse voltammetry (DPV) experiments were performed using a CH Instruments CHI760E potentiostat. A three-electrode setup consisted of a glassy carbon working electrode (3.0 mm disk), a Pt wire auxiliary electrode, and a standard Ag/AgCl reference electrode. Cyclic voltammograms were recorded at scan rates of 10−100 mV s^{-1} and were let run for at least ten full cycles. The 20 mM phosphate buffer solution (pH 7) containing 1 mM $Mg(OAc)_2$ (used in the AuNC synthesis) was the only electrolyte source. Differential pulse voltammograms were obtained at a pulse period of 250 ms, pulse width of 25 ms, amplitude of 25 mV, and increment of 2 mV. All sample solutions were first deoxygenated and then blanketed with an argon atmosphere throughout the CV and DPV experiments.

Electrochemical Measurements for ORR. *1. Preparation of BOD-AuNC/SWNT Composite Materials.* First, a suspension of 1% single-walled carbon nanotubes (SWNT, cheaptubes.com) in 4:1 water:methanol solution and 0.1% tetrabutylammonium bromide (TBAB)-modified Nafion (provided by Prof. Shelley Minteer, University of Utah) in absolute ethanol was made and bath sonicated for 30 min at RT to disperse the SWNT. Five μL of the AuNC solution was added to 40 μL of the SWNT-TBAB-Nafion suspension and left for 1 h to allow for the stacking of the DNA to the SWNT. Identical luminescence emission spectra of the AuNC before and after mixing with SWNT-TBAB-Nafion confirmed that the integrity of the AuNC remained intact after stacking with SWNT (Figure S9). Next, 2 μL (4 mg/mL) 1-pyrenebutanoic acid succinimidyl ester (PBSE, Sigma-Aldrich) dissolved in ethanol were introduced to the SWNT-TBAB-Nafion-AuNC mixture and incubated for additional 1 h. After the PBSE adsorption on the SWNT, 2 μL of a 200 mg/mL BOD (Amano Enzyme Inc.) solution in 100 mM phosphate buffer at pH 7.5 was added and the sample was incubated for 16−18 h at 4 °C. The BOD-AuNC/SWNT composite material thus prepared was further used for the ORR experiments. Controls consisting of BOD/SWNT, BOD-DNA/SWNT, and BOD-plasmonic Au/SWNT were prepared using same procedure. The concentration of DNA in the composites was estimated according to suitable dilutions from the DNA concentration in the respective precursor materials, as determined using an extinction coefficient of 2.78 × 10^5 M^{-1} cm^{-1} provided by IDT.

A glassy carbon rotating disk electrode (RDE) (disk area 0.2475 cm^2, Pine Instruments) was used. The RDE was cleaned with alumina of increasingly fine grits of 1, 0.3, and 0.05 mm, and rinsed with deionized water. After cleaning the electrode, 10 μL of SWNT-TBAB-Nafion suspension were dropped on the electrode surface and dried under a flow of N_2 gas. Next, 10 μL of the composite material (BOD/SWNT, BOD-DNA/SWNT, BOD-plasmonic Au/SWNT or BOD-AuNC/SWNT) was drop cast on the RDE and allowed to air-dry before the electrochemical measurements.

2. Preparation of MWBP Electrode. Circular pieces (0.3 mm diameter) of MWBP were cut, immersed in a solution of the AuNC, and left for 1 h for attachment of the AuNC with MWBP. The paper discs were then washed with DI water and transferred to a 10 mM solution of PBSE in ethanol. After 1 h, the modified nanotube paper was washed with DI water and placed in solution of BOD (10 mg/mL in 100 mM phosphate buffer, pH 7.5) and incubated at 4 °C for 18 h. After enzyme immobilization, the electrodes were washed again with buffer to remove any unattached enzyme. The modified MWBP discs were then placed on a glassy carbon cap electrode and tested in 100 mM phosphate buffer, pH 7.5. A control electrode was prepared the same way except for the use of AuNC.

3. Electrocatalytic Measurements. RDE measurements were performed with a WEB30 Pine bipotentiostat and a rotator from Pine Instruments. A three-electrode setup (glassy carbon working electrode, Pt wire auxiliary electrode, Ag/AgCl reference electrode) was used. The electrolyte was a 100 mM phosphate buffer solution at pH 7.5. Enough time (20 min) was allowed for the system at open circuit conditions to reach equilibrium. Using linear sweep voltammetry (LSV) the disk potential was swept from 0.8 to 0 V at a scan rate of 10 mV/s. At least three sets of independent ORR data were collected from three different preparations of composite samples as well as controls. With each preparation, the ORR currents were measured in electrolyte solutions containing dissolved O_2, saturated O_2 (purged for 20 min), and depleted O_2 (N_2 purged for 20 min). Potentiostatic polarization curves of the BOD-AuNC/MWBP and BOD/MWBP electrodes were carried out by applying a constant potential for 300 s, starting from open-circuit potential to 0 V vs Ag/AgCl, with a step increase of 0.05 V. Potentials measured against Ag/AgCl ($E^0_{Ag/AgCl}$ = 0.197 V) were converted to RHE using[58]

$$E_{RHE} = E_{Ag/AgCl} + 0.059 \times pH + E^0_{Ag/AgCl}$$

4. Oxygen Reduction Reaction Current. The electrochemical current (Δi) was calculated by determining the difference in the reductive current at ∼0.300 V vs Ag/AgCl (0.940 V vs RHE) and the current at the onset potential for oxygen reduction.

5. Mass and Charge Balance Analysis Using RRDE. For the mass and charge balance analysis using rotating ring disk electrode (RRDE), the BOD-AuNC/SWNT composite was drop cast on electrode surface, dried, and the ORR activity was measured in 100 mM phosphate buffer at pH 7.5. Using a bipotentiostat (Pine Instruments), the disk current was swept from 0.800 to 0 V at a scan rate of 10 mV/s while the ring was polarized at 0.800 V. Data analysis was performed according to eq 1.

■ ASSOCIATED CONTENT

Supporting Information

The Supporting Information is available free of charge on the ACS Publications website at DOI: 10.1021/jacs.5b05338.

MALDI-MS, EDX, N 1s XPS, lifetime measurements, effect of $NaBH_4$ on luminescence, effect of DNA concentration on electrocatalytic current density, RRDE data, and the effect of SNWT on the luminescence of AuNC. (PDF)

■ AUTHOR INFORMATION

Corresponding Authors

*plamen@unm.edu

*jenm@lanl.gov

Present Address

⊥Department of Chemistry, Colorado State University, Fort Collins, Colorado 80523, United States.

Author Contributions

‖S.C. and S.B. contributed equally.

Notes

The authors declare no competing financial interest.

■ ACKNOWLEDGMENTS

The authors would like to acknowledge financial support by the Laboratory Directed Research and Development (LDRD) program for EDX and TEM (A.D.), synthesis, photophysics, and electrochemistry by the Basic Energy Sciences, Biomolecular Materials Program, Division of Materials Science & Engineering (S.C., R.C.R., J.S.M.). P.A. thanks the Air Force

Office of Scientific Research (Grant FA9550-12-1-0112) and ARO-Multi-University Research Initiative grant W911NF-14-1-0263 to University of Utah for funding this collaborative project. This work was performed, in part, at the Center for Integrated Nanotechnologies, an Office of Science User Facility operated for the U.S. Department of Energy (DOE) Office of Science. Los Alamos National Laboratory, an affirmative action equal opportunity employer, is operated by Los Alamos National Security, LLC, for the National Nuclear Security Administration of the U.S. Department of Energy under contract DE-AC52-06NA25396. The authors thank Dr. Darrick Williams for helping with EDX data collection, and Timothy Sanchez for helping with MALDI data collection.

REFERENCES

(1) (a) Qiao, Y.; Li, C. M. *J. Mater. Chem.* **2011**, *21*, 4027−4036. (b) Zhou, M.; Wang, J. *Electroanalysis* **2012**, *24*, 197−209. (c) Zebda, A.; Gondran, C.; Le Goff, A.; Holzinger, M.; Cinquin, P.; Cosnier, S. *Nat. Commun.* **2011**, *2*, 370. (d) Holzinger, M.; Le Goff, A.; Cosnier, S. *Electrochim. Acta* **2012**, *82*, 179−190. (e) Katz, E.; MacVittie, K. *Energy Environ. Sci.* **2013**, *6*, 2791−2803. (f) Halámková, L.; Halámek, J.; Bocharova, V.; Szczupak, A.; Alfonta, L.; Katz, E. *J. Am. Chem. Soc.* **2012**, *134*, 5040−5043. (g) Zafar, M. N.; Beden, N.; Leech, D.; Sygmund, C.; Ludwig, R.; Gorton, L. *Anal. Bioanal. Chem.* **2012**, *402*, 2069−2077. (h) Harreither, W.; Felice, A. K.; Paukner, R.; Gorton, L.; Ludwig, R.; Sygmund, C. *Biotechnol. J.* **2012**, *7*, 1359−1366. (i) Jia, W.; Valdés-Ramírez, G.; Bandodkar, A. J.; Windmiller, J. R.; Wang, J. *Angew. Chem., Int. Ed.* **2013**, *52*, 7233−7236. (j) Chen, X.; Li, C.; Grätzel, M.; Kostecki, R.; Mao, S. S. *Chem. Soc. Rev.* **2012**, *41*, 7909−7937.

(2) (a) Davis, F.; Higson, S. P. *Biosens. Bioelectron.* **2007**, *22*, 1224−1235. (b) Minteer, S. D.; Liaw, B. Y.; Cooney, M. J. *Curr. Opin. Biotechnol.* **2007**, *18*, 228−234. (c) Bullen, R. A.; Arnot, T.; Lakeman, J.; Walsh, F. *Biosens. Bioelectron.* **2006**, *21*, 2015−2045.

(3) Aricò, A. S.; Bruce, P.; Scrosati, B.; Tarascon, J.-M.; Van Schalkwijk, W. *Nat. Mater.* **2005**, *4*, 366−377.

(4) Holland, J. T.; Lau, C.; Brozik, S.; Atanassov, P.; Banta, S. *J. Am. Chem. Soc.* **2011**, *133*, 19262−19265.

(5) (a) Shang, L.; Dong, S.; Nienhaus, G. U. *Nano Today* **2011**, *6*, 401−418. (b) Lin, C.-A. J.; Lee, C.-H.; Hsieh, J.-T.; Wang, H.-H.; Li, J. K.; Shen, J.-L.; Chan, W.-H.; Yeh, H.-I.; Chang, W. H. *J. Med. Biol. Eng.* **2009**, *29*, 276−283. (c) Lin, C.-A. J.; Yang, T.-Y.; Lee, C.-H.; Huang, S. H.; Sperling, R. A.; Zanella, M.; Li, J. K.; Shen, J.-L.; Wang, H.-H.; Yeh, H.-I.; Parak, W. J.; Chang, W. H. *ACS Nano* **2009**, *3*, 395−401. (d) Li, G.; Jin, R. *Acc. Chem. Res.* **2013**, *46*, 1749−1758. (e) Wilcoxon, J.; Abrams, B. *Chem. Soc. Rev.* **2006**, *35*, 1162−1194. (f) Link, S.; Beeby, A.; FitzGerald, S.; El-Sayed, M. A.; Schaaff, T. G.; Whetten, R. L. *J. Phys. Chem. B* **2002**, *106*, 3410−3415. (g) Proch, S.; Wirth, M.; White, H. S.; Anderson, S. L. *J. Am. Chem. Soc.* **2013**, *135*, 3073−3086.

(6) (a) Murray, R. W. *Chem. Rev.* **2008**, *108*, 2688−2720. (b) Walter, M.; Akola, J.; Lopez-Acevedo, O.; Jadzinsky, P. D.; Calero, G.; Ackerson, C. J.; Whetten, R. L.; Grönbeck, H.; Häkkinen, H. *Proc. Natl. Acad. Sci. U. S. A.* **2008**, *105*, 9157−9162. (c) Jadzinsky, P. D.; Calero, G.; Ackerson, C. J.; Bushnell, D. A.; Kornberg, R. D. *Science* **2007**, *318*, 430−433. (d) Zeng, C.; Qian, H.; Li, T.; Li, G.; Rosi, N. L.; Yoon, B.; Barnett, R. N.; Whetten, R. L.; Landman, U.; Jin, R. *Angew. Chem.* **2012**, *124*, 13291−13295. (e) Lee, D.; Donkers, R. L.; Wang, G.; Harper, A. S.; Murray, R. W. *J. Am. Chem. Soc.* **2004**, *126*, 6193−6199.

(7) Hammer, B.; Norskov, J. *Nature* **1995**, *376*, 238−240.

(8) (a) Haruta, M.; Daté, M. *Appl. Catal., A* **2001**, *222*, 427−437. (b) Haruta, M. *Catal. Today* **1997**, *36*, 153−166.

(9) (a) Boccuzzi, F.; Cerrato, G.; Pinna, F.; Strukul, G. *J. Phys. Chem. B* **1998**, *102*, 5733−5736. (b) Hayden, B. E.; Pletcher, D.; Suchsland, J. P. *Angew. Chem., Int. Ed.* **2007**, *46*, 3530−3532. (c) Valden, M.; Lai, X.; Goodman, D. W. *Science* **1998**, *281*, 1647−1650. (d) Hernández, J.; Solla-Gullón, J.; Herrero, E.; Aldaz, A.; Feliu, J. M. *J. Phys. Chem. C* **2007**, *111*, 14078−14083. (e) Mohr, C.; Hofmeister, H.; Radnik, J.; Claus, P. *J. Am. Chem. Soc.* **2003**, *125*, 1905−1911. (f) Hughes, M. D.; Xu, Y.-J.; Jenkins, P.; McMorn, P.; Landon, P.; Enache, D. I.; Carley, A. F.; Attard, G. A.; Hutchings, G. J.; King, F.; Stitt, E. H.; Johnston, P.; Griffin, K.; Kiely, C. J. *Nature* **2005**, *437*, 1132−1135.

(10) van Bokhoven, J. A.; Miller, J. T. *J. Phys. Chem. C* **2007**, *111*, 9245−9249.

(11) Tang, W.; Lin, H.; Kleiman-Shwarsctein, A.; Stucky, G. D.; McFarland, E. W. *J. Phys. Chem. C* **2008**, *112*, 10515−10519.

(12) Herzing, A. A.; Kiely, C. J.; Carley, A. F.; Landon, P.; Hutchings, G. J. *Science* **2008**, *321*, 1331−1335.

(13) (a) Zhu, Y.; Qian, H.; Zhu, M.; Jin, R. *Adv. Mater.* **2010**, *22*, 1915−1920. (b) Liu, Y.; Tsunoyama, H.; Akita, T.; Xie, S.; Tsukuda, T. *ACS Catal.* **2010**, *1*, 2−6. (c) Xie, S.; Tsunoyama, H.; Kurashige, W.; Negishi, Y.; Tsukuda, T. *ACS Catal.* **2012**, *2*, 1519−1523.

(14) Zhu, Y.; Qian, H.; Drake, B. A.; Jin, R. *Angew. Chem., Int. Ed.* **2010**, *49*, 1295−1298.

(15) Kauffman, D. R.; Alfonso, D.; Matranga, C.; Qian, H.; Jin, R. *J. Am. Chem. Soc.* **2012**, *134*, 10237−10243.

(16) Chen, W.; Chen, S. *Angew. Chem., Int. Ed.* **2009**, *48*, 4386−4389.

(17) (a) Wu, Z.; Jin, R. *Nano Lett.* **2010**, *10*, 2568−2573. (b) Xie, J.; Zheng, Y.; Ying, J. Y. *J. Am. Chem. Soc.* **2009**, *31*, 888−889.

(18) (a) Petty, J. T.; Zheng, J.; Hud, N. V.; Dickson, R. M. *J. Am. Chem. Soc.* **2004**, *126*, 5207−5212. (b) Zheng, J.; Nicovich, P. R.; Dickson, R. M. *Annu. Rev. Phys. Chem.* **2007**, *58*, 409−431. (c) O'Neill, P. R.; Velazquez, L. R.; Dunn, D. G.; Gwinn, E. G.; Fygenson, D. K. *J. Phys. Chem. C* **2009**, *113*, 4229−4233. (d) Schultz, D.; Gwinn, E. G. *Chem. Commun.* **2012**, *48*, 5748−5750. (e) Sharma, J.; Rocha, R. C.; Phipps, M. L.; Yeh, H. C.; Balatsky, K. A.; Vu, D. M.; Shreve, A. P.; Werner, J. H.; Martinez, J. S. *Nanoscale* **2012**, *4*, 4107−4110. (f) Sharma, J.; Yeh, H.-C.; Yoo, H.; Werner, J. H.; Martinez, J. S. *Chem. Commun.* **2010**, *46*, 3280−3282. (g) Yeh, H. C.; Sharma, J.; Han, J. J.; Martinez, J. S.; Werner, J. H. *Nano Lett.* **2010**, *10*, 3106−3110.

(19) Jia, X.; Li, J.; Han, L.; Ren, J.; Yang, X.; Wang, E. *ACS Nano* **2012**, *6*, 3311−3317.

(20) (a) Seidel, R.; Colombi Ciacchi, L.; Weigel, M.; Pompe, W.; Mertig, M. *J. Phys. Chem. B* **2004**, *108*, 10801−10811. (b) Tiwari, J. N.; Nath, K.; Kumar, S.; Tiwari, R. N.; Kemp, K. C.; Le, N. H.; Youn, D. H.; Lee, J. S.; Kim, K. S. *Nat. Commun.* **2013**, *4*, 2221.

(21) Zhu, Y.; Qian, H.; Jin, R. *J. Mater. Chem.* **2011**, *21*, 6793.

(22) (a) Pinheiro, A. V.; Han, D.; Shih, W. M.; Yan, H. *Nat. Nanotechnol.* **2011**, *6*, 763−772. (b) Seeman, N. C. *Mol. Biotechnol.* **2007**, *37*, 246−257.

(23) Mertig, M.; Colombi Ciacchi, L.; Seidel, R.; Pompe, W.; De Vita, A. *Nano Lett.* **2002**, *2*, 841−844.

(24) (a) Kennedy, T. A.; MacLean, J. L.; Liu, J. *Chem. Commun.* **2012**, *48*, 6845−6847. (b) Liu, G.; Shao, Y.; Ma, K.; Cui, Q.; Wu, F.; Xu, S. *Gold Bull.* **2012**, *45*, 69−74. (c) Liu, G.; Shao, Y.; Wu, F.; Xu, S.; Peng, J.; Liu, L. *Nanotechnology* **2013**, *24*, 015503.

(25) (a) Solomon, E. I.; Heppner, D. E.; Johnston, E. M.; Ginsbach, J. W.; Cirera, J.; Qayyum, M.; Kieber-Emmons, M. T.; Kjaergaard, C. H.; Hadt, R. G.; Tian, L. *Chem. Rev.* **2014**, *114*, 3659−3853. (b) Liu, J.; Chakraborty, S.; Hosseinzadeh, P.; Yu, Y.; Tian, S.; Petrik, I.; Bhagi, A.; Lu, Y. *Chem. Rev.* **2014**, *114*, 4366−4469.

(26) Ivnitski, D. M.; Khripin, C.; Luckarift, H. R.; Johnson, G. R.; Atanassov, P. *Electrochim. Acta* **2010**, *55*, 7385−7393.

(27) (a) Luo, Z.; Yuan, X.; Yu, Y.; Zhang, Q.; Leong, D. T.; Lee, J. Y.; Xie, J. *J. Am. Chem. Soc.* **2012**, *134*, 16662−16670. (b) Negishi, Y.; Nobusada, K.; Tsukuda, T. *J. Am. Chem. Soc.* **2005**, *127*, 5261−5270.

(28) Yang, Y.; Chen, S. *Nano Lett.* **2003**, *3*, 75−79.

(29) (a) Menard, L. D.; Xu, H.; Gao, S.-P.; Twesten, R. D.; Harper, A. S.; Song, Y.; Wang, G.; Douglas, A. D.; Yang, J. C.; Frenkel, A. I. *J. Phys. Chem. B* **2006**, *110*, 14564−14573. (b) Menard, L. D.; Gao, S.-P.; Xu, H.; Twesten, R. D.; Harper, A. S.; Song, Y.; Wang, G.; Douglas, A. D.; Yang, J. C.; Frenkel, A. I. *J. Phys. Chem. B* **2006**, *110*, 12874−12883.

(30) Zheng, J.; Petty, J. T.; Dickson, R. M. *J. Am. Chem. Soc.* **2003**, *125*, 7780−7781.

DOI: 10.1021/jacs.5b05338
J. Am. Chem. Soc. 2015, 137, 11678−11687

(31) (a) Jaw, H. R. C.; Mason, W. R. *Inorg. Chem.* **1991**, *30*, 275−278. (b) Hall, K. P.; Theoblad, B. R. C.; Gilmour, D. I.; Mingos, D. M. P.; Welch, A. J. *J. Chem. Soc., Chem. Commun.* **1982**, 528−530. (c) Bartlett, P. A.; Bauer, B.; Singer, S. *J. Am. Chem. Soc.* **1978**, *100*, 5085−5089.
(32) Zheng, J.; Zhang, C.; Dickson, R. M. *Phys. Rev. Lett.* **2004**, *93*, 077402.
(33) (a) Ramasamy, P.; Guha, S.; Shibu, E. S.; Sreeprasad, T. S.; Bag, S.; Banerjee, A.; Pradeep, T. *J. Mater. Chem.* **2009**, *19*, 8456−8462. (b) Levi-Kalisman, Y.; Jadzinsky, P. D.; Kalisman, N.; Tsunoyama, H.; Tsukuda, T.; Bushnell, D. A.; Kornberg, R. D. *J. Am. Chem. Soc.* **2011**, *133*, 2976−2982.
(34) Qian, H.; Jin, R. *Chem. Mater.* **2011**, *23*, 2209−2217.
(35) Petty, J. T.; Fan, C.; Story, S. P.; Sengupta, B.; Iyer, A. S.; Prudowsky, Z.; Dickson, R. M. *J. Phys. Chem. Lett.* **2010**, *1*, 2524−2529.
(36) (a) Santiago Gonzalez, B.; Rodriguez, M. J.; Blanco, C.; Rivas, J.; Lopez-Quintela, M. A.; Gaspar Martinho, J. M. *Nano Lett.* **2010**, *10*, 4217−4221. (b) Guliamov, O.; Frenkel, A. I.; Menard, L. D.; Nuzzo, R. G.; Kronik, L. *J. Am. Chem. Soc.* **2007**, *129*, 10978−10979.
(37) (a) Sengupta, B.; Ritchie, C. M.; Buckman, J. G.; Johnsen, K. R.; Goodwin, P. M.; Petty, J. T. *J. Phys. Chem. C* **2008**, *112*, 18776−18782. (b) Ritchie, C. M.; Johnsen, K. R.; Kiser, J. R.; Antoku, Y.; Dickson, R. M.; Petty, J. T. *J. Phys. Chem. C* **2007**, *111*, 175−181. (c) Neidig, M. L.; Sharma, J.; Yeh, H.-C.; Martinez, J. S.; Conradson, S. D.; Shreve, A. P. *J. Am. Chem. Soc.* **2011**, *133*, 11837−11839. (d) Duguid, J.; Bloomfield, V. A.; Benevides, J.; Thomas, G. J., Jr *Biophys. J.* **1993**, *65*, 1916.
(38) (a) Yam, V. W. W.; Cheng, E. C. C.; Zhou, Z. Y. *Angew. Chem., Int. Ed.* **2000**, *39*, 1683−1685. (b) White-Morris, R. L.; Olmstead, M. M.; Jiang, F.; Tinti, D. S.; Balch, A. L. *J. Am. Chem. Soc.* **2002**, *124*, 2327−2336. (c) Cha, S.-H.; Kim, J.-U.; Kim, K.-H.; Lee, J.-C. *Chem. Mater.* **2007**, *19*, 6297−6303.
(39) Brouwer, A. M. *Pure Appl. Chem.* **2011**, *83*, 2213−2228.
(40) Huang, T.; Murray, R. W. *J. Phys. Chem. B* **2001**, *105*, 12498−12502.
(41) Negishi, Y.; Tsukuda, T. *Chem. Phys. Lett.* **2004**, *383*, 161−165.
(42) Bigioni, T.; Whetten, R.; Dag, Ö. *J. Phys. Chem. B* **2000**, *104*, 6983−6986.
(43) Chen, S.; Wang, S.; Zhong, J.; Song, Y.; Zhang, J.; Sheng, H.; Pei, Y.; Zhu, M. *Angew. Chem., Int. Ed.* **2015**, *54*, 3145−3149.
(44) Garcia-Raya, D.; Madueno, R.; Blazquez, M.; Pineda, T. *J. Phys. Chem. C* **2009**, *113*, 8756−8761.
(45) Qian, H.; Zhu, Y.; Jin, R. *ACS Nano* **2009**, *3*, 3795−3803.
(46) Nimmala, P. R.; Yoon, B.; Whetten, R. L.; Landman, U.; Dass, A. *J. Phys. Chem. A* **2013**, *117*, 504−517.
(47) Zanello, P. *Inorganic Electrochemistry: Theory, Practice, and Application*; Royal Society of Chemistry, Cambridge, U.K., 2003.
(48) Moore, C. M.; Akers, N. L.; Hill, A. D.; Johnson, Z. C.; Minteer, S. D. *Biomacromolecules* **2004**, *5*, 1241−1247.
(49) Gupta, G.; Lau, C.; Rajendran, V.; Colon, F.; Branch, B.; Ivnitski, D.; Atanassov, P. *Electrochem. Commun.* **2011**, *13*, 247−249.
(50) Shleev, S.; El Kasmi, A.; Ruzgas, T.; Gorton, L. *Electrochem. Commun.* **2004**, *6*, 934−939.
(51) (a) Ramasamy, R. P.; Luckarift, H. R.; Ivnitski, D. M.; Atanassov, P. B.; Johnson, G. R. *Chem. Commun.* **2010**, *46*, 6045−6047. (b) Weigel, M. C.; Tritscher, E.; Lisdat, F. *Electrochem. Commun.* **2007**, *9*, 689−693.
(52) Wang, C.; Daimon, H.; Onodera, T.; Koda, T.; Sun, S. *Angew. Chem., Int. Ed.* **2008**, *47*, 3588−3591.
(53) (a) Chen, Z.; Waje, M.; Li, W.; Yan, Y. *Angew. Chem., Int. Ed.* **2007**, *46*, 4060−4063. (b) Seo, M. H.; Choi, S. M.; Kim, H. J.; Kim, W. B. *Electrochem. Commun.* **2011**, *13*, 182−185. (c) Lim, B.; Jiang, M.; Camargo, P. H.; Cho, E. C.; Tao, J.; Lu, X.; Zhu, Y.; Xia, Y. *Science* **2009**, *324*, 1302−1305.
(54) Liang, Y.; Li, Y.; Wang, H.; Zhou, J.; Wang, J.; Regier, T.; Dai, H. *Nat. Mater.* **2011**, *10*, 780−786.
(55) (a) Hsueh, K. L.; Chin, D. T.; Srinivasan, S. *J. Electroanal. Chem. Interfacial Electrochem.* **1983**, *153*, 79−95. (b) Brett, C. M. A.; Brett, A. M. O. *Electrochemistry Principles, Methods and Applications*; Oxford University Press, Inc.: New York, NY, 1993.
(56) Brocato, S.; Lau, C.; Atanassov, P. *Electrochim. Acta* **2012**, *61*, 44−49.
(57) Williams, A. T. R.; Winfield, S. A.; Miller, J. N. *Analyst* **1983**, *108*, 1067−1071.
(58) Bard, A. J.; Faulkner, L. R. *Electrochemical Methods: Fundamentals and Applications*; Wiley: New York, 1980; Vol. *2*.

DOI: 10.1021/jacs.5b05338
J. Am. Chem. Soc. 2015, 137, 11678−11687